CHEMISTRY OF MATERIALS
Article

*Chem. Mater.* **2010,** *22,* 6301–6309 6301
DOI:10.1021/cm102069w

# Hyperbranched Polymers for the Formation and Stabilization of ZnO Nanoparticles

Sarmenio Saliba,[†,‡,§] Clara Valverde Serrano,[†,‡] Juliane Keilitz,[⊥] Myrtil L. Kahn,*[,†,§] Christophe Mingotaud,[†,‡] Rainer Haag,[⊥] and Jean-Daniel Marty*[,†,‡]

[†]*University of Toulouse, 118 route de Narbonne, 31062 Toulouse, France,* [‡]*Laboratoire IMRCP, CNRS UMR 5623, 31062 Toulouse, France,* [§]*Laboratoire de Chimie de Coordination, CNRS UPR 8241, 31062 Toulouse, France, and* [⊥]*Department of Chemistry & Biochemistry, Freie Universität Berlin, Takustrasse 3, 14195 Berlin, Germany*

*Received July 26, 2010. Revised Manuscript Received October 10, 2010*

The synthesis and characterization of a new family of dendritic polymers comprising a hyperbranched polyamidoamine core and polyethyleneglycol-derivative units is reported. The mentioned polymers have either core−shell or core−multishell architectures. Their intrinsic properties (solubility in a wide range of solvents, ability to interact with hydrophilic or hydrophobic compounds, etc.) allows the one-step in situ synthesis of water-soluble ZnO quantum dots via decomposition of an organometallic precursor. The effect of structural properties of the polymer (nature of the shell, core molecular weight, etc.), as well as external stimuli (temperature, ionic strength, etc.) on the formation and/or stabilization of nanoparticles has been evaluated. The as-synthesized nanoparticles could be easily redispersed in various solvents and presented stable photoluminescent properties.

## 1. Introduction

Luminescent inorganic nanoparticles, better known as quantum dots (QDs), have been used for important applications in the biomedical sector.[1] Because of their small size, these materials undergo a quantum confinement effect and benefit from exceptional properties not present in the bulk systems. In fact, QDs are known for their sharp emissions, high quantum yields, and size-dependent tunable emission wavelengths over a wide spectrum.[1a,2] Also, cost-effective QDs are nowadays more sought-after than conventional organic fluorophores in imaging research, which are more sensitive to photo bleaching. Until now, cadmium based II−VI semiconductors were by far the most promising materials. Despite their intriguing properties, examples such as CdSe and CdTe have been reported as toxic to biological media. The toxicity is generally linked to several factors including release of cadmium salts upon exposure to UV radiation or aging.[3] Other studies have shown that Cd QDs can cause toxicity via photoinduced reactive oxygen species (ROS) generation. Surface chemistry can also play an important role in nanoparticles (NPs) toxicity and therefore other phenomena such as charge transfer and surface oxidation have to be taken into account.[4] Nowadays, QD research is increasingly focused on the challenge of synthesizing biologically- and eco-friendly light-emitting nanoparticles. For utmost biological exploitation, such nanoparticles should possess a small diameter,[5] high quantum yields, and long-term stable photoluminescence in saline water. ZnO is a well-known wide-gap semiconductor with a band gap value of 3.37 eV at room temperature that displays luminescent properties in the near UV and visible regions of the spectrum. As well as being inexpensive, it has been frequently reported to be nontoxic to living cells and possesses antimicrobial properties.[3a,6] Therefore, we can consider ZnO as an ideal biofriendly substitute for Cd-based semiconductors in biological labeling. A number of reports account for ZnO QDs prepared via sol−gel routes.[7] However, the stated synthesis generally requires heating conditions which limit morphological control at the nanometric scale. Sol−gel-derived nanoparticles also tend to have poor colloidal and photophysical stability in aqueous media. To bypass these problems, our group has previously reported the synthesis of ZnO nanoparticles through the decomposition of an organo-metallic precursor.[8] It has been shown that the

*Corresponding author. E-mail: marty@chimie.ups-tlse.fr (J.-D.M.); myrtil.kahn@lcc-toulouse.fr (M.L.K.). Tel: 33 561-556-135 (J.-D.M.); 33 561-333-130 (M.L.K.). Fax: 33 561-558-155 (J.-D.M.).

(1) (a) Bruchez, M.; Moronne, M.; Gin, P.; Weiss, S.; Alivisatos, A. P. *Science* **1998**, *281*(5385), 2013–2016. (b) Jaiswal, J. K.; Mattoussi, H.; Mauro, J. M.; Simon, S. M. *Nat. Biotechnol.* **2003**, *21*(1), 47–51. (c) Michalet, X.; Pinaud, F. F.; Bentolila, L. A.; Tsay, J. M.; Doose, S.; Li, J. J.; Sundaresan, G.; Wu, A. M.; Gambhir, S. S.; Weiss, S. *Science* **2005**, *307*(5709), 538–544.
(2) Chan, W. C. W.; Nie, S. M. *Science* **1998**, *281*(5385), 2016–2018.
(3) (a) Wu, Y. L.; Lim, C. S.; Fu, S.; Tok, A. I. Y.; Lau, H. M.; Boey, F. Y. C.; Zeng, X. T. *Nanotechnology* **2007**, *18*(21), 9. (b) Derfus, A. M.; Chan, W. C. W.; Bhatia, S. N. *Nano Lett.* **2004**, *4*(1), 11–18.
(4) (a) Dumas, E.; Gao, C.; Suffern, D.; Bradforth, S. E.; Dimitrijevic, N. M.; Nadeau, J. L. *Environ. Sci. Technol.* **2010**, *44*(4), 1464–1470. (b) Schneider, R.; Wolpert, C.; Guilloteau, H.; Balan, L.; Lambert, J.; Merlin, C. Nanotechnology **2009**, *20* (22), 225101.
(5) Hillaireau, H.; Couvreur, P. *Cell. Mol. Life Sci.* **2009**, *66*(17), 2873–2896.
(6) Padmavathy, N.; Vijayaraghavan, R. *Sci. Technol. Adv. Mater.* **2008**, *9*(3), 035004.
(7) Sanchez, C.; Soler-Illia, G.; Ribot, F.; Lalot, T.; Mayer, C. R.; Cabuil, V. *Chem. Mater.* **2001**, *13*(10), 3061–3083.


Published on Web 11/08/2010

latter approach provides improved chemical versatility and better control of nanoparticle morphology. However, two main drawbacks are generally found with the fabrication of ZnO through such a process. The first is the necessity to use specific solvents and ligand molecules, if the morphology of the particle is to be well-controlled. The second is related to the nonfacile surface modification of the obtained NPs (by ligand exchange for example). A great challenge nowadays is the development of alternative methods that provide convenient access to ligand-functionalized ZnO NPs. Especially attractive is the free choice of the organic shell according to the specific desired properties of the final product, without limiting factors related to the NP synthetic conditions.

To date, only a handful of reports discuss water-stable ZnO NPs that are small-sized and biocompatible. Fu et al. have reported a route for the synthesis of stable aqueous ZnO nanoparticles with strong blue emission from zinc nitrate and oleic acid (OA) in diethanolamine solution.[9] The blue emission is suggested to be a result of surface-bound OA molecules, while the water stability is provided by the hydroxyl groups at the surface. Despite interesting photoluminescent properties useful in color displays and other electronic devices, the mentioned nanohybrids are less applicable to bioimaging techniques, since biological cells generally also emit blue light upon UV irradiation. Moreover, due to the nature of the protecting shell, this material was sensitive to changes in pH or ionic strength. To introduce biocompatibility to ZnO NPs, Xiong et al. have proposed a copolymer shell-protected ZnO NPs synthesized in an anhydrous solvent via a sol−gel method.[10] The copolymer shell comprises an inner hydrophobic polymethacrylate layer and an outer hydrophilic polyethyleneglycol shell, allowing easy redispersibility in aqueous solutions and ensuring colloidal stability. In contrast to Fu and co-workers, these QDs emit in the green and yellow regions of the spectrum and have been successfully tested as fluorescent probes for in vitro imaging. Other authors have successfully used silane-based functionalized polymers as stabilizing agent for ZnO NPs in water.[11] Jana and co-workers have described the formation of ZnO nanocrystals from a solution of zinc acetate and oleic acid in ethanol under reflux, after which a modification of the surface was carried out by a two-step silanization process. This functionalization allowed the grafting of charged functional groups upon a silane protective shell, thus providing colloidal stability in water. Moussodia and co-workers have also reported the formation of water-soluble ZnO QDs of around 6 nm in diameter. The synthesis of ZnO was performed via a precipitation method using oleic acid as capping agent in ethanol, followed by a cap exchange with PEG-siloxane in order to achieve hydrophilicity.[11b] This capping agent, however, lacks surface groups that can be conjugated with bioactive molecules, leading to ZnO materials with low potential for use in bioapplications. Recent work carried out by Tang et al. describes a two-step synthesis of water-soluble ZnO QDs. In a first step, ZnO NPs were prepared via a precipitation method with lithium hydroxide in ethanol. The second step involved the encapsulation of these NPs with silica in order to provide stability in aqueous media. The advantage of this work is that the as-synthesized ZnO NP emission could be tuned by changing the pH of the precipitate solution.[12]

More recently, ZnO nanohybrids involving dendritic capping agents have gained special interest.[13] They are characterized by their three-dimensional molecular shapes and present a large number of functional end groups, which makes them easy to tailor for end-user purposes. Moreover, several intriguing properties such as high reactivity, good compatibility with other materials, high solubility and low viscosity compared with their linear counterparts, have been described.[14] Hence, dendrimers have been used as "nano-reactors" in which metal cations can complex with the internal heteroatoms. Reduction leads to stabilized nanoparticles with sizes of only a few nanometers, which is presumably related to the given space within the structure.[14a] Dendrimers have also been used to stabilize and control the growth of nanoclusters by forming inter-dendrimer complexes, resulting in larger metal nanoclusters protected by terminal amine groups.[14a] Hence, Moussodia and co-workers have functionalized preformed oleate-capped ZnO QDs with siloxane-core PAMAM dendrons.[13a] Because of the branched nature of dendrimers and the presence of multivalent surface groups, this system seems to be more appealing for biological labeling. The QDs produced have a desired particle size of around 5 nm and a relatively good quantum yield in water. In contrast to perfectly branched monodisperse dendrimers, randomly branched (i.e., hyperbranched) polymers are easily accessible (they are less costly than dendrimers and can be synthesized on a large scale) and they often have equivalent properties to their dendritic counterparts. Hyperbranched polymers have been reported to effectively stabilize metallic NPs in organic solvents or in water.[15,16] Recently, Ludwigs and co-workers have

(8) Monge, M.; Kahn, M. L.; Maisonnat, A.; Chaudret, B. *Angew. Chem., Int. Ed.* **2003**, *42*(43), 5321–5324.
(9) Fu, Y. S.; Du, X. W.; Kulinich, S. A.; Qiu, J. S.; Qin, W. J.; Li, R.; Sun, J.; Liu, J. *J. Am. Chem. Soc.* **2007**, *129*(51), 16029–16033.
(10) Xiong, H. M.; Xu, Y.; Ren, O. G.; Xia, Y. Y. *J. Am. Chem. Soc.* **2008**, *130*(24), 7522–7523.
(11) (a) Jana, N. R.; Yu, H. H.; Ali, E. M.; Zheng, Y. G.; Ying, J. Y. *Chem. Commun.* **2007**, No. 14, 1406–1408. (b) Moussodia, R. O.; Balan, L.; Schneider, R. *New J. Chem.* **2008**, *32*(8), 1388–1393.
(12) Tang, X. S.; Choo, E. S. G.; Li, L.; Ding, J.; Xue, J. M. *Chem. Mater.* **2010**, *22*(11), 3383–3388.
(13) (a) Moussodia, R. O.; Balan, L.; Merlin, C.; Mustin, C.; Schneider, R. *J. Mater. Chem.* **2010**, *20*(6), 1147–1155. (b) Richter, T. V.; Schuler, F.; Thomann, R.; Mulhaupt, R.; Ludwigs, S. *Macromol. Rapid Commun.* **2009**, *30*(8), 579–583.
(14) (a) Scott, R. W. J.; Wilson, O. M.; Crooks, R. M. *J. Phys. Chem. B* **2005**, *109*(2), 692–704. (b) Vohs, J. K.; Fahlman, B. D. *New J. Chem.* **2007**, *31*(7), 1041–1051.
(15) (a) Garcia-Bernabé, A.; Krämer, M.; Olàh, B.; Haag, R. *Chem.—Eur. J.* **2004**, *10*, 2822–2830. (b) Lu, Y.; Mei, Y.; Walker, R.; Ballauf, M.; Drechsler, M. *Polymer* **2006**, *47*, 4985–4995. (c) Mecking, S.; Thomann, R.; Frey, H.; Sunder, A. *Macromolecules* **2000**, *33*, 3958–3960. (d) Monticelli, O.; Russo, S.; Campagna, R.; Voit, B. *Polymer* **2005**, No. 46, 3597–3606. (e) Schlotterbeck, U.; Aymonier, C.; Thomann, R.; Hofmeister, H.; Tromp, M.; Richtering, W.; Mecking, S. *Adv. Funct. Mater.* **2004**, *14*(12), 999–1004. (f) Tabuani, D.; Monticelli, O.; Chincarini, A.; Bianchini, C.; Vizza, F.; Moneti, S.; Russo, S. *Macromolecules* **2003**, *36*(12), 4294–4301.

**Scheme 1. Schematic Structure of HYPAM Polymer with a Double- or Single-Shell Structure; HYPAM$_x$ Corresponds to a Hyperbranched Polymer with Various Molecular Weight**

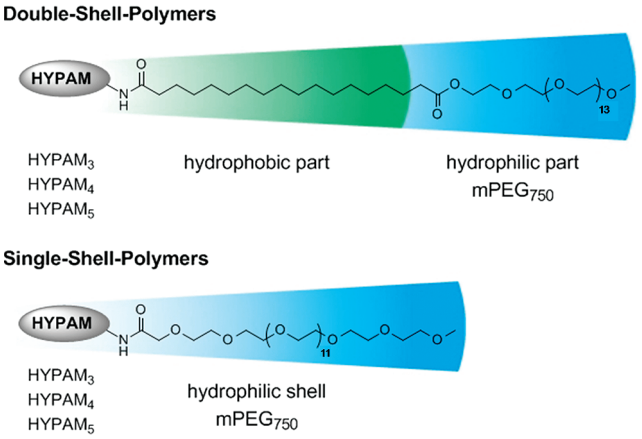


prepared hyperbranched polyether polyol-ZnO nanohybrids by slow decomposition of $Zn(C_2H_5)_2$ in air. The polymer was made amphiphilic by partial stearate modification.[13b] The hybrid exhibited interesting luminescent properties, however its dispersibility was limited to apolar solvents.

Most reports mentioned above concerning the formation of water-soluble ZnO NPs, require multistep synthesis. This normally involves the preformation of ZnO nanocrystals using a primary capping agent, which is then replaced by water-compatible stabilizing agent for aqueous transfer. Moreover, nanohybrids with core−shell structures appear to be better stabilizing agents; the inner shell (generally hydrophobic) helps prevent the loss of photoluminescence in aqueous media, whereas the hydrophilic outer shell confers stabilization properties in water. Hence, a straightforward synthesis for the production of long-term water stable ZnO NPs is still a well soughtafter target. Here we report the one-step in situ synthesis of ZnO QDs, using an organometallic precursor, stabilized by hyperbranched polymers (HBPs) based on core-multishell architectures. Primarily, the synthesis and characterization of a new family of dendritic polymers comprising a hyperbranched polyamidoamine core and a polyethyleneglycol-based shell is described (Scheme 1). Then, this specific architecture (core−shell or core−multishell) was utilized for the one-step formation of water-soluble ZnO nanohybrids. The effect of structural properties of the polymer (nature of the shell, core molecular weight, etc.), as well as external stimuli (temperature and, ionic strength, etc.) on the formation, stabilization, and photoluminescence properties of nanoparticles have been evaluated.

(16) (a) Perignon, N.; Mingotaud, A. F.; Marty, J. D.; Rico-Lattes, I.; Mingotaud, C. Chem. Mater. **2004**, *16*, (24), 4856-+ (b) Kramer, M.; Perignon, N.; Haag, R.; Marty, J. D.; Thomann, R.; Lauth-de Viguerie, N.; Mingotaud, C. *Macromolecules* **2005**, *38*(20), 8308–8315. (c) Perignon, N.; Marty, J. D.; Mingotaud, A. F.; Dumont, M.; Rico-Lattes, I.; Mingotaud, C. *Macromolecules* **2007**, *40*(9), 3034–3041. (d) Keilitz, J.; Radowski, M. R.; Marty, J. D.; Haag, R.; Gauffre, F.; Mingotaud, C. *Chem. Mater.* **2008**, *20*(7), 2423–2425. (e) Marty, J. D.; Martinez-Aripe, E.; Mingotaud, A. F.; Mingotaud, C. *J. Colloid Interface Sci.* **2008**, *326*(1), 51–54. (f) Keilitz, J.; Nowag, S.; Marty, J. D.; Haag, R. *Adv. Synth. Catal.* **2010**, *352*(9), 1503–1511.

## 2. Experimental Section

**2.1. Materials.** Tris(2-aminoethyl)amine (Aldrich) was distilled under reduced pressure and stored under argon atmosphere before use. Tris(2-di(methylacrylate)aminoethyl)amine (MA6-TREN) was synthesized according to the method described by Dvornic.[17] Zinc precursor [$Zn(Cy)_2$] was purchased from NANOMEPS. Unless otherwise stated, all other chemicals have been used as provided from the suppliers (Acros, Fluka, or Aldrich). Water content was systematically measured by Karl Fischer coulometric titration on a Metrohm instrument. Sensitive substances and reactions were handled in a MBraun Inert Gas System or under an argon atmosphere in carefully dried glassware, using standard Schlenk techniques. Organic layers were dried using magnesium sulfate, min. 99.5% (Sigma-Aldrich). Silica gel 60 (Merck, 230−240 mesh) was used for column chromatography. Benzoylated Dialysis Tubing with average flat 32 mm MWCO 1000 was obtained from Sigma-Aldrich.

**2.2. Characterization.** To determine the structural characteristics of the polymers, $^1$H NMR and $^{13}$C NMR spectra were recorded on a Bruker ARX 500 equipped with a cryogenic probe and a Bruker ECX 400 (400 MHz for $^1$H and 100 MHz for $^{13}$C). Calibration was performed using the chloroform peak at 7.26 ppm for $^1$H and 77.0 ppm for $^{13}$C. IR spectra were recorded on KBr plates on a Nicolet Avator 320 FT-IR spectrometer. The molecular weight of the polymers was determined by size exclusion chromatography (SEC) analysis on an apparatus equipped with a Waters refractive index detector, and a Minidawn Wyatt light scattering detector. Analyses were performed either in carbonate buffer solution at pH 10 with a Waters column pack (Shodex OHpak SB-802HQ, SB-802.5HQ, SB-804HQ) or in THF with a Waters column pack (Ultrastyragel $10^4$, $10^3$, 100 Å). The molecular weights were uncorrected from low sensitivity of LS-SEC to lower molecular weights. The refractive index increments for PAMAM dendrimers were measured in the same eluent at ambient temperature. The values for the hyperbranched polyamides core were assumed to be identical. Considering the fact that these polymers have been observed to trap solvent molecules, even after prolonged drying under vacuum, the accuracy of the molecular weight measurements were estimated to be around 20%. The temperatures at which glass transitions ($T_g$) and crystallizations ($T_c$) occur were determined by Differential Scanning Calorimetry (DSC) using a Perkin-Elmer PYRIS 1 calorimeter. $T_c$ was taken to be the temperature at the top of the DSC peaks as the temperature decreased at different rates; 40, 20, 10, and 5 °C/min, and finally extrapolated to 0 °C/min. $T_g$ was measured as the temperature increased at a rate of 10 °C/min.

To study aggregation properties of the hyperbranched polymer in aqueous solutions, we performed surface tension experiments using the pending-drop technique (KRÜSS instrument, model DSA10-Mk2). The solutions were prepared by dissolving a precise weight of surfactant [using a Sartorius microbalance Genius model (±0.05 mg)] in a defined volume of water. DLS measurements were carried out with a Malvern Instrument Nano-ZS equipped with a He−Ne laser ($\lambda$ = 633 nm). The correlation function was analyzed via the general purpose method (NNLS) to obtain the distribution of diffusion coefficients ($D$) of the solutes. The apparent equivalent hydrodynamic diameter ($\langle D_h \rangle$) was then determined using the Stokes−Einstein equation. Mean diameter values were obtained from three different runs. Standard deviations were evaluated from diameter distribution. Besides scattering measurements, the morphology of the obtained

(17) Dvornic, P. R.; Hu, J.; Meier, D. J.; Nowak, R. M.; Parham, P. L. U.S. 2002/0161113 A1, 2002.

nanohybrids was studied by transmission electron microscopy (TEM). TEM was performed on a JEOL 120 kV electronic microscope. A drop of the aqueous dispersion was placed on a carbon-coated 200 mesh copper TEM grid (Ted Pella Inc.) and left to dry in air. For samples needing negative staining, the TEM grid was successively placed on a drop of the sample solution for 2 min, on a drop of an aqueous solution of uranyl acetate (2 wt %, 2 min) and finally on a drop of distilled water, after which the grid was then air-dried before introduction into the electron microscope. At least 200 particles were analyzed (using the WCIF ImageJ software) for the calculation of mean diameter and standard deviation. Emission spectra were recorded using a PTI spectrometer equipped with a Xenon lamp. An HP 8452A diode array spectrometer was used for absorption spectra recording (optical path length: 1 cm).

**2.3. Synthesis.** *2.3.1. Double- and Single-Shell Synthesis*. The general synthesis of double-shell building block **mPEG$_{750}$-C$_{17}$-COOH** (**1**) has been described before.[18] Briefly, 1 equiv. of mPEG$_{750}$-OH, 4 equiv. of 1,18-octadecanedioic acid, and 2.5 mol % *p*-toluenesulphonic acid (PTSA) in toluene were stirred under reflux in a flask equipped with a Dean−Stark trap for 24 h. The solution was then cooled down to 0 °C, the excess of diacid was filtered off and the mixture concentrated by removal of the solvent. Purification was achieved by flash chromatography with a gradient $CHCl_3$:MeOH 10:0 to 10:1 (v:v) as eluent. The single-shell building block **mPEG$_{750}$-COOH** (**2**) was prepared by oxidation with Jones Reagent adapting a procedure published elsewhere.[19] Typically, 20 g of mPEG$_{750}$−OH was dissolved in 200 mL of acetone, 48.6 mL of Jones reagent (8.99 g of $CrO_3$ dissolved in 64.20 mL of water and the solution cooled to 10 °C; 7.80 mL of concentrated $H_2SO_4$ was added dropwise under stirring and the mixture was allowed to reach room temperature) was added, and the solution was stirred at room temperature over 20 h. The reaction was quenched by addition of 5 mL of isopropanol. The crude product was concentrated and purified by silica gel column chromatography performed with a 95:5 (v:v) $CHCl_3$:$Et_3N$ mixture and using a gradient eluent of $CHCl_3$:MeOH from 99:1 to 90:10 (v:v). 6.41 g of pure mPEG$_{750}$-COOH was recovered (Yield: 34%).

$^1$H NMR (400 MHz, $CDCl_3$) $\delta$: 4.01 (s, O-*$CH_2$*-COOH); 3.80−3.44 (m large, PEG backbone); 3.35 (s, -O-*$CH_3$*); 3.04 (q, $Et_3N$ traces: N(*$CH_2$*-$CH_3$)$_3$); 1.25 (t, $Et_3N$ traces: N($CH_2$-*$CH_3$*)$_3$). $^{13}$C NMR (100 MHz, $CDCl_3$) $\delta$: 174.19 (-O-$CH_2$-*COOH*); 71.86 (-*$CH_2$*-O-$CH_3$); 70.49 (br *PEG*); 70.00 (-O-*$CH_2$*-COOH); 58.95 (-O-*$CH_3$*) ppm.

*2.3.2. Preparation of Hyperbranched Polyamidoamine Cores*. The hyperbranched polymers were prepared as already described.[16a,c] Taking HYPAM$_5$ as an example, 2.44 g of tris-(2-aminoethyl)amine (16.7 mmol) was mixed with 1.42 g of MA6-TREN (2.14 mmol). The solution was stirred under argon at 70 °C for 2 days, after which the products were dissolved in 5 mL $CH_2Cl_2$ and precipitated into 200 mL of THF at 0 °C. 2.37 g of precipitated polymer was obtained as a yellow gum.

$^1$H NMR (400 MHz, $CDCl_3$) $\delta$: 2.1−2.9 (m, -*$NH_2$*, -*$CH_2$*-$NH_2$, -*$CH_2$*-CO-); 3.25 (br m, -*$CH_2$*-NHCO-); 8.29 (br s, -NHCO−). $^1$H NMR (400 MHz, $D_2O$) $\delta$: 2.34 (m, -$CH_2$-CO-); 2.5 (m, N-*$CH_2$*-*$CH_2$*-N); 2.55 (m, CONH-$CH_2$-*$CH_2$*-N); 2.63 (m, -*$CH_2$*-$NH_2$); 2.73 (m, N-*$CH_2$*-$CH_2$−CO); 3.22 (m, -*$CH_2$*-NHCO−) ppm.

$^{13}$C NMR (100 MHz, $D_2O$) $\delta$: 32.6, 35.5 (-*$CH_2$*-CO); 36.7 (-*$CH_2$*-NH-CO-); 37.8 (-*$CH_2$*-$NH_2$); 49.1 (N-*$CH_2$*-$CH_2$-CO); 49.8, 51.1, 52.5 (CONH-$CH_2$-*$CH_2$*-N); 56.0 (N-*$CH_2$*-*$CH_2$*-N); 174.5 (*CONH*) ppm.

*2.3.3. Grafting of PEG$_{750}$-C$_{17}$-COOH or PEG$_{750}$-COOH on the HYPAM core*. *N*-Hydroxysuccinimide (SuOH) (1 equiv.) and *N*,*N*′-dicyclohexylcarbodiimide (DCC) (1.05 equiv.) were added to 1 equiv. of (**1**) or (**2**) in THF. The mixture was stirred at room temperature for 12−20 h, kept at 50 °C overnight to crystallize 1,3-dicyclohexylurea (DCU) and filtrated. This procedure was repeated several times until no more DCU visibly crystallized. The solvent was removed in vacuo and the obtained shell building blocks (**3**) and (**4**) were used without further purification. For coupling, the shell building block (1.05 equiv.) was added to the hyperbranched core (1 equiv. of $NH_2$ groups) in methanol and stirred for 24 h at room temperature. The resulting core−(multi)shell structures were purified by dialysis in methanol for 3 days with three solvent changes.

*HYPAM$_x$-PEG$_{750}$*. HYPAM$_3$-PEG$_{750}$: $^1$H NMR (400 MHz, MeOD-d4) $\delta$: 3.70−3.57 (br, -O-*$CH_2$*-*$CH_2$*-O- from mPEG); 3.34 (s, -O-*$CH_3$* from mPEG); 3.28−3.20 (br, -CO-NH-*$CH_2$*-); 2.84−2.75 (br, N-*$CH_2$*-$CH_2$-CO); 2.73−2.69 (br, $NH_2$-*$CH_2$*-); 2.67−2.56 (br, N-*$CH_2$*-$CH_2$-NH-CO); 2.55−2.48 (br, N-*$CH_2$*-*$CH_2$*-N-); 2.45−2.35 (br, -*$CH_2$*-CO-) ppm.

HYPAM$_4$-PEG$_{750}$ and HYPAM$_5$-PEG$_{750}$: $^1$H NMR (400 MHz, $D_2O$) $\delta$: 3.71 (br, -O-*$CH_2$*-*$CH_2$*-O- from mPEG); 3.34 (s, -O-*$CH_3$* from mPEG); (3.39 (br, -CO-NH-*$CH_2$*-); 2.79 (br, N-*$CH_2$*-$CH_2$-CO); 2.79 (br, $NH_2$-*$CH_2$*-); 2.67 (br, N-*$CH_2$*-$CH_2$-NH-CO); 2.67 (br, N-$CH_2$-$CH_2$-N-); 2.45 (br, -*$CH_2$*-CO-) ppm.

$^{13}$C NMR (100 MHz, $D_2O$) $\delta$: 174.5 (-NH-*CO*-$CH_2$ from HYPAM core and core-shell link); 71.02 (-*$CH_2$*-O-$CH_3$); 69.7 (-O-*$CH_2$*-$CH_2$−O); 60.4 (-O-*$CH_3$*); 58.1 (NH-CO-$CH_2$-*$CH_2$*-O); 51.4−53.6 (N-*$CH_2$*-*$CH_2$*-N and CONH-*$CH_2$*-*$CH_2$*-N); 52.4, 49.2−50.3 (N-*$CH_2$*-$CH_2$-CO); 37.1 (CO-NH-*$CH_2$*- $CH_2$-O) ppm.

IR (KBr): $\bar{\nu}$(cm$^{-1}$) = 1107, 1539, 1644, 1733, 3428.

*HYPAM$_x$-C$_{18}$−PEG$_{750}$*. HYPAM$_3$-C$_{18}$-PEG$_{750}$: $^1$H NMR (400 MHz, $CDCl_3$) $\delta$: 4.19 (t, -COO-*$CH_2$*); 3.67−3.53 (br, -O-*$CH_2$*-*$CH_2$*-O- from mPEG); 3.35 (s, -O-*$CH_3$* from mPEG); 3.22 (br -CO-NH-*$CH_2$*-); 2.70 (br, CO-NH-$CH_2$-*$CH_2$*-N- and NHCO-$CH_2$-*$CH_2$*-N- from HYPAM); 2.52 (br, -N-*$CH_2$*-*$CH_2$*-N- and -NH-*$CH_2$*-*$CH_2$*-NH- from HYPAM); 2.29 (t, -*$CH_2$*-COO−); 2.19 (br, NHCO*$CH_2$* from core−shell link); 2.14 (m, NHCO*$CH_2$* from HYPAM); 1.58 (br, NHCO-$CH_2$-*$CH_2$*-$(CH_2)_{12}$-*$CH_2$*-$CH_2$-COO); 1.21 (m, NHCO-$CH_2$-$CH_2$−$(CH_2)_{12}$-$CH_2$-$CH_2$-COO-) ppm.

HYPAM$_4$-C$_{18}$−PEG$_{750}$: $^1$H NMR (400 MHz, $CDCl_3$) $\delta$: 4.18 (t, -COO-*$CH_2$*); 3.82−3.40 (br, -O-*$CH_2$*-*$CH_2$*-O- from mPEG); 3.35 (s, -O-*$CH_3$*); 3.21 (br, -CO-NH-*$CH_2$*-); 2.69 (br, CO-NH-$CH_2$-*$CH_2$*-N- from NHCO-$CH_2$-*$CH_2$*-N- from HYPAM); 2.52 (br, -N-*$CH_2$*-*$CH_2$*-N- and -NH-*$CH_2$*-*$CH_2$*-NH- from HYPAM); 2.30 (t, -*$CH_2$*-COO-); 2.19 (br, NHCO*$CH_2$*); 1.58 (br, NHCO-$CH_2$-*$CH_2$*-$(CH_2)_{12}$-*$CH_2$*-$CH_2$-COO); 1.21 (m, NHCO-$CH_2$-$CH_2$-$(CH_2)_{12}$-$CH_2$-$CH_2$−COO−) ppm.

HYPAM$_5$-C$_{18}$-PEG$_{750}$: $^1$H NMR (400 MHz, $CDCl_3$) $\delta$: 3.80−3.32 (-O-*$CH_2$*-*$CH_2$*-O- from mPEG); 3.34 (s, -O-*$CH_3$*); 2.13 (t, $CH_2$*$CH_2$*COOH, and $CH_2$*$CH_2$*CONH); 1.55 (m, *$CH_2$*$CH_2$COOH and *$CH_2$*$CH_2$CONH); 1.22 (m, 12H, -$(CH_2)_6$-) ppm.

$^{13}$C NMR (100 MHz, $CDCl_3$) $\delta$: 174.1 (−NH-*CO*-$CH_2$ from HYPAM core and core−shell link); 173.7 -$CH_2$-*COO*-); 71.9 (-*$CH_2$*-O-$CH_3$); 70.5 (-O-*$CH_2$*-*$CH_2$*-O); 69.1 (-COO-$CH_2$-*$CH_2$*-); 63.3 (-COO-*$CH_2$*); 58.9 (-O-*$CH_3$*); 53.4 − 55.1 (N-*$CH_2$*-*$CH_2$*-N); 51.1−52.4 (CONH−$CH_2$-*$CH_2$*-N); 49.4−50.6 (N-*$CH_2$*-$CH_2$-CO); 37.6 (−CO-NH-*$CH_2$*-$CH_2$−N-); 36.4 (CO-NH-*$CH_2$*- from the core−shell link); 34.1 (NH-CO-*$CH_2$*); 28.8−30.9

(18) Radowski, M. R.; Shukla, A.; von Berlepsch, H.; Bottcher, C.; Pickaert, G.; Rehage, H.; Haag, R. *Angew. Chem., Int. Ed.* **2007**, *46* (8), 1265–1269.
(19) Lele, B. S.; Kulkarni, M. G. *J. Appl. Polym. Sci.* **1998**, *70*(5), 883–890.

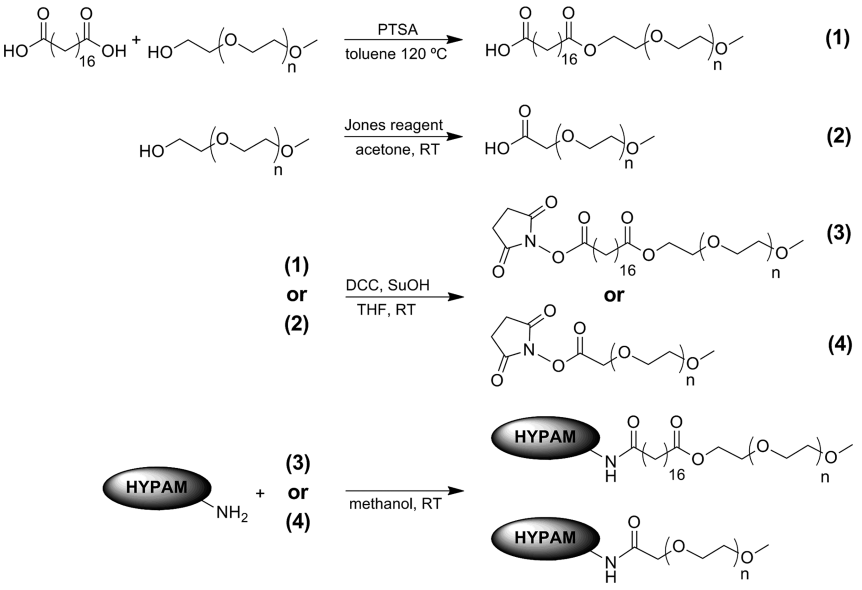


**Figure 1.** Synthesis of HYPAM-based hyperbranched polymers with a single or double shell.

(NHCO-$CH_2$-$CH_2$-($CH_2$)$_{12}$-$CH_2$-$CH_2$-COO-); 25.9 (-NH-CO-$CH_2$-$CH_2$-); 24.8 (-$CH_2$-$CH_2$-COO-) ppm.

IR (KBr): $\bar{\nu}$(cm$^{-1}$) = 1032, 1530, 1644, 3280.

*2.3.4. Formation of ZnO Nanoparticles.* Synthesis of ZnO/hyperbranched polymer (HBP) hybrids was carried out as follows. A solution of HBP in predried THF (approximately 30 ppm of water) was prepared under an argon atmosphere (concentration: $1.4 \times 10^{-4}$ mol L$^{-1}$). Three mL aliquots of HBP solution were then transferred to a Schlenk tube followed by the addition of the desired quantity of dicyclohexyl zinc ([Zn(Cy)$_2$]) precursor. The solution was left to stir for 15 min under inert conditions. The mixtures were subsequently exposed to ambient moisture, generally for a period of two days. During this time the solvent evaporated leaving behind a white luminescent residue of ZnO nanoparticles.

## 3. Results and Discussion

**3.1. Synthesis and Characterization of Hyperbranched Polymers.** Different families of HBP were elaborated. The synthesis of hyperbranched polymers core (noted HYPAM) with a similar structure as PAMAM dendrimers was based on the reaction of a hexaester with a trisamine. This method has the advantage to lead to the hyperbranched structure in a single step and can be carried out in large quantities. Its main drawback is to give polymers with broad molecular weight distributions. The molecular weight of the polymers was easily adjusted by changing the ratio between the triamine and the hexaester. Molar ratios close to 12:1, 10:1, or 8:1 led to polymers with molecular weight close to those of PAMAM of the third, fourth, and fifth generation, respectively.[16a] These hyperbranched polymers were therefore named HYPAM$_3$, HYPAM$_4$ or HYPAM$_5$. The HYPAM cores of different molecular weight were then functionalized with linear hydrophilic or amphiphilic building blocks formed by alkyl diacids ($C_0$ or $C_{18}$) connected to monomethyl poly(ethylene glycol) (mPEG$_{750}$: PEG with 14 glycol units on average). The attachment of the single or double shell was carried out according to an already published procedure with hyperbranched PEI polymers (Figure 1).[18] Briefly, the carboxylic acid function of PEG$_{750}$-$C_{17}$-COOH or mPEG$_{750}$-COOH were activated using dicyclohexyl-carbodiimide (DCC) as coupling agent and then reacted with primary amino groups. These were functionalized quantitatively as demonstrated by $^1$H NMR- (see the Supporting Information, Figure S1).

The molecular weight of HYPAM derivatives was evaluated by size exclusion chromatography (SEC) in a carbonate buffer at a pH of 10. The analysis of hyperbranched polymers by SEC has been the subject of many articles.[20] Because of the peculiar architecture, a regular analysis with standard calibration is not valid. The use of a light scattering and refractometric detector, allows an evaluation of the molecular weight of the polymers. However, even with this approach, for wide distributions, the difference of sensitivity of light scattering between high and low molecular weights leads to an underestimated polydispersity index. Some authors have proposed a method to compensate for this effect.[20c] In our case, this correction led to an increase in the polydispersity index only for unmodified HYPAM samples (from 2.2 to 4.9 for HYPAM$_5$). However, if the use of this program is relevant for regular linear polymers, it might not be adequate for hyperbranched structures, because some interactions between the polymer and the column might still be present besides size exclusion. Therefore, the molecular weight and dispersity indices presented in Table 1 are not corrected. Furthermore, these polymers have been observed to trap solvent molecules even after prolonged drying. Thus, the measured molecular weight should be considered as indicative values. It is noteworthy that values of molecular weights obtained for PAMAM dendrimers in similar chromatographic conditions were consistent with the expected values.[16c] Grafting of the single shell induced an

(20) (a) Hong, L.; Wang, X.; Tang, X. *J. Appl. Polym. Sci.* **2002**, *85*, 2445–2450. (b) Kunamaneni, S.; Buzza, D. M.; Parker, D.; Feast, W. J. *J. Mater. Chem.* **2003**, *13*, 2749–2755. (c) Zagar, E.; Zigon, M. *Macromolecules* **2002**, *35*, 9913–9925.

**Table 1. Properties of Investigated Polymers**

| | | | thermal properties[c] | |
|---|---|---|---|---|
| | $\overline{M_w}$[a] | Đ[b] | $T_g$ (°C) ($\Delta C_p$ (J/g)) | $T_f$ (°C) ($\Delta H$ (J/(g °C))) |
| $HYPAM_3$ | 4800 | 1.3 | −31 (0.9) | |
| $HYPAM_3$-$PEG_{750}$ | 25000 | 1.4 | | 18.0 (28) |
| $HYPAM_3$-$C_{18}$-$PEG_{750}$ | n.r. | | | 41.5 (86) |
| $HYPAM_4$ | 9800 | 1.4 | −9.0 (0.5) | |
| $HYPAM_4$-$PEG_{750}$ | 39000 | 1.5 | | 23.4 (33) |
| $HYPAM_4$-$C_{18}$-$PEG_{750}$ | n.r. | | | 44.8 (82) |
| $HYPAM_5$ | 13800 | 2.2 | −7.6 (0.8) | |
| $HYPAM_5$-$PEG_{750}$ | 95000 | 1.9 | | |
| $HYPAM_5$-$C_{18}$-$PEG_{750}$ | n.r. | | | 43.0 (64) |

[a] Molecular weight determined by LS-SEC. [b] Dispersity index determined by SEC. [c] Thermal properties obtained from DSC measurements. Glass transition temperatures $T_g$ were given at a heating rate of 10 °C/min and fusion temperatures $T_f$ were obtained from maximum peak values extrapolated at 0 °C/min. n.r. = not reported because of aggregation phenomenon.

increase of molecular weights compatible with the expected theoretical value estimated from quantitative modification of primary terminal amino groups (see Table 1). Nevertheless, in the case of HBP with a double shell structure, such analysis could not be properly performed. Hence, aggregation phenomenon occurring in water (vide infra) induced a strong overestimation of the molecular weight.

Differential scanning calorimetry (DSC) analyses were performed for all polymers. Figure 2 shows the thermograms obtained for $HYPAM_4$, $HYPAM_4$-$PEG_{750}$ and $HYPAM_4$-$C_{18}$-$PEG_{750}$. They showed a transition temperature at around −9.0 °C for $HYPAM_4$ polymer that could be attributed to a glass transition temperature. This transition was no more visible when the HYPAM core was grafted with a single or a double shell. Instead an endothermic peak (with increasing associated enthalpy variation) appears at 18.0 and 41.5 °C for $HYPAM_4$-$PEG_{750}$ and $HYPAM_4$-$C_{18}$-$PEG_{750}$, respectively. A similar trend was also observed for $HYPAM_3$ and $HYPAM_5$ based hyperbranched polymers (see Table 1). Therefore, in bulk, these polymers tend to organize at a molecular level. As this process was greatly enhanced by the presence of the hydrophobic shell, this suggests the existence of alkyl/alkyl or PEG/PEG interactions.

*Aggregation Properties in Water*. When amphiphilic block copolymers are dissolved in water, they tend to aggregate in order to decrease the Gibbs free energy of the system by the formation of an "interface" between "oily" cores and water (the so-called hydrophobic effect).[21] The aggregation properties for HYPAM-based hyperbranched polymers in water were analyzed by surface-tension measurements on a pendant drop apparatus as a function of concentration (for a range between ca. $1 \times 10^{-4}$ and 2 g $L^{-1}$). The surface tension was found to decrease to values of 50 mN $m^{-1}$, a surface activity that is typical for amphiphilic systems. An abrupt change in the slope of the curves is also observed, suggesting the possibility of an aggregation phenomenon occurring between individual structures in solution. However, because of the very slow kinetics of the polymer systems its value was found to depend on the way the polymer solution was prepared. To further confirm the previous findings, we have carried out DLS measurements on $HYPAM_4$-$C_{18}$−$PEG_{750}$ polymer in solution. For dilute conditions (0.021 g $L^{-1}$), scattering intensities corresponding to an almost monomodal distribution of objects with a hydrodynamic diameter of around 9 nm were recorded. This value is in good agreement with the size of the unimolecular hyperbranched polymers.[18] Upon increasing concentration (above 0.1 g $L^{-1}$), a new population intensity signal corresponding to objects of around 30 nm was observed. This bimodal distribution confirms the existence of unimolecular HYPAM-multishell architectures and their aggregates in solution. The exact aggregated structure is not known, however this aggregation phenomenon may be similar to the one reported by Radowski et al.,[18] on shell-protected dendritic structures. The same DLS experiments were also carried out using THF, the solvent used during ZnO NPs synthesis (vide infra). The hydrodynamic radius of objects present in solution, for dilute conditions (for example 0.042 g $L^{-1}$), was found to be around 13 nm. When the concentration was increased (up to 1.4 g $L^{-1}$), the size distribution in number corresponded to one major population of small object of around 13 nm. However, the distribution intensity signal for objects between 10 and 50 nm was observed. Hence, for such concentrations, a minor aggregated population of HBP is also present in THF.

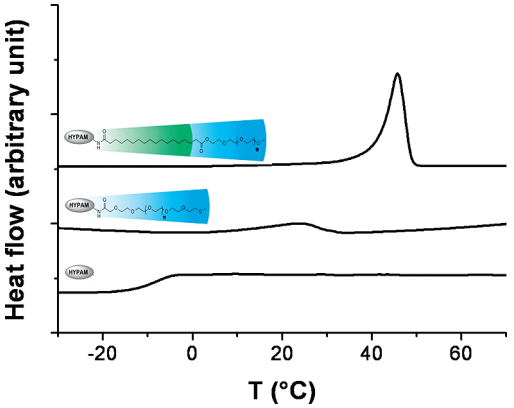


**Figure 2.** DSC thermograms for $HYPAM_4$, $HYPAM_4$-$PEG_{750}$, and $HYPAM_4$-$C_{18}$-$PEG_{750}$ at a heating rate of 10 °C/min.

**3.2. Synthesis of ZnO NPs.** Formation of ZnO nanoparticles was performed via a one-step hydrolysis of dicyclohexyl zinc ($[Zn(Cy)_2]$) precursor in THF. This method generally involves the use of long alkyl chain amine ligands as stabilizers and takes advantage of the exothermic reaction commonly displayed by organometallic complexes in air.[8] Using $[Zn(Cy)_2]$ as a precursor provides a safer synthetic method than other organometallic complexes such as diethyl zinc, used by Richter and co-workers and is a precursor whose hydrolysis is more easily controllable.[13b] Control over the kinetics of ZnO formation was ensured by the interactions occurring between amino ligands and $[Zn(Cy)_2]$ or ZnO NPs and has been reported to have direct effects on the chemical versatility of the synthesized ZnO NPs.[22] In the case of $HYPAM_x$-$C_{18}$−$PEG_{750}$, the presence of multiple amino groups in the polymeric core should

(21) Chandler, D. *Nature* **2005**, *437*(7059), 640–647.

guarantee interactions with [Zn(Cy)$_2$] (and ZnO NPs). Moreover, the inner hydrophobic shell should favor the solubilization of the hydrophobic [Zn(Cy)$_2$] precursor in the hyperbranched structure and act as a protective layer for ZnO NPs in water. The terminal PEG chains not only act as an external polar layer providing good solubility in water and organic solvents, but also improve the biocompatibility of the hybrid.

The introduction of the zinc precursor into the HYPAM system is achieved in THF. The HYPAM core alone is insoluble in THF and therefore cannot be used as a host for the growth of NPs. HYPAM-single shell structures of the type HYPAM$_x$-PEG$_{750}$ are soluble in polar solvents but less soluble in apolar ones. These solubility properties limit the quantity of [Zn(Cy)$_2$] precursor that can be added to the system. This therefore led us to structures of a double-shell nature: HYPAM$_x$-C$_{18}$−PEG$_{750}$. The latter, because of its amphiphilic nature, is easily solubilized in both polar and apolar solvents, making it a potential candidate for the stabilization of ZnO NPs. Several mixtures containing varying weight ratios of zinc precursor to polymer were prepared in dry THF (HYPAM$_x$-C$_{18}$-PEG$_{750}$/[Zn(Cy)$_2$]: 1/1.7, 1/1.2, 1/0.4), under an argon atmosphere. These ratios were chosen in order to have an excess of amine (primary, secondary, or tertiary amines or amide groups) per molecule of [Zn(Cy)$_2$] precursor[16c] and to avoid the presence of free precursor agent in solution that could induce the formation of ZnO large aggregates during the hydrolysis step. In the case of HYPAM$_4$-C$_{18}$-PEG$_{750}$ this corresponds to [amine]/ [Zn(Cy)$_2$] molar ratios of 1.6, 2.4, and 7.2, respectively. Interactions between the zinc precursor and the hyperbranched polymer host were assessed by $^1$H NMR experiments (Figure 3). A mixture of [Zn(Cy)$_2$] (1.8 mg, 0.008 mmol), and HYPAM$_3$-C$_{18}$-PEG$_{750}$ (600 $\mu$L of a 1.4 g·L$^{-1}$ THF-d8 solution) was prepared under an inert atmosphere inside a sealable NMR tube (weight ratio HYPAM$_3$-C$_{18}$-PEG$_{750}$/[Zn(Cy)$_2$] = 1/0.4, molar ratio amine/[Zn(Cy)$_2$] = 3.6). From $^1$H NMR spectra, we could observe that all signals corresponding to protons in proximity to a nitrogen atom, show a widely broadened or diminished signal in presence of the zinc precursor (see Figure 3, spectrum 1 and 2). On the other hand, the rest of the signals arising from protons in the multishell architectures remained unaltered. This means that in the prehydrolysis state, the zinc atoms interact with nitrogen atoms localized in the HYPAM core rather than in the surrounding hydrophobic shell. The broadening of signals occurs because of fluxionality hindrance upon interaction with the organometallic precursor. The higher this interaction is, the broader is the signal, up to a point where the signal is no longer visible. The NMR tube containing the reaction mixture was then opened to the atmosphere allowing the hydrolysis of [Zn(Cy)$_2$] to proceed. This process leads to the formation of luminescent ZnO NPs a few hours after. $^1$H NMR results are presented in Figure 3, Spectrum 3. After hydrolysis takes place in air,

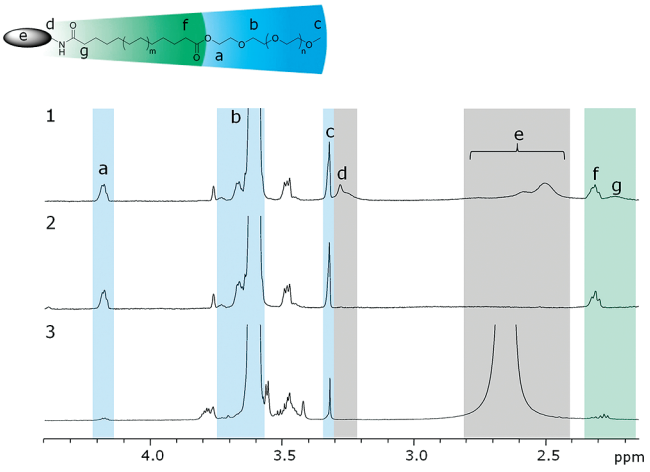


**Figure 3.** $^1$H-NMR spectra for (1) HYPAM$_3$-C$_{18}$-PEG$_{750}$; (2) mixture of HYPAM$_3$-C$_{18}$-PEG$_{750}$/[Zn(Cy)$_2$]; and (3) HYPAM$_3$-C$_{18}$-PEG$_{750}$/ZnO. Polymer/[Zn(Cy)$_2$] ratio used: 1/2.1, in 600 $\mu$L THF-d8 as solvent. Proton signal assignment; [Color code: gray - protons in the core; green - protons in the hydrophobic shell; blue - protons in the PEG shell]; (a) −COO−*CH*$_2$, (b) −O−*CH*$_2$−*CH*$_2$−O− from mPEG and signal from THF-d8, (c) −O−*CH*$_3$ from mPEG, (d) −CO−NH−*CH*$_2$−, (e) CO−NH−CH$_2$−*CH*$_2$−N−, NHCO−CH$_2$−*CH*$_2$-N−, −N−*CH*$_2$−*CH*$_2$−N− and −NH−*CH*$_2$−*CH*$_2$−NH− from HYPAM, (f) −*CH*$_2$−COO−, (g) NHCO*CH*$_2$ from core−shell link. Large signal at 2.64 ppm in spectrum 3 is assigned to water. The spectra highlight the key effects of the presence of [Zn(Cy)$_2$] and ZnO NPs on the hyperbranched polymer.

a signal corresponding to water protons appears at 2.65 ppm. Whereas nitrogen-neighboring protons remain invisible, a significant decrease in signal intensity for protons in the PEG shell was also observed. Hence, this bottom-up organometallic approach leads to nucleation and growth of ZnO nanoparticles that then became surrounded by HBP.

The synthesized ZnO NPs were further analyzed by transmission electron microscopy (TEM). Samples were prepared by dropcasting a solution of the composite in THF onto a copper-coated grid. Taking HYPAM$_3$ as an example, the size of the NPs ranged from 4.5 ± 0.7 nm to 3.7 ± 0.7 nm for a polymer/[Zn(Cy)$_2$] weight ratio of 1/1.7 and 1/0.4, respectively (see Figure 4a). Therefore, for a given polymer, variation of [Zn(Cy)$_2$] quantity revealed a small effect on the size of the particles. The size obtained from TEM micrographs was further evaluated using the Meulenkamp equation.[23] As reported by Meulenkamp, the wavelength at which the absorption is half that of the excitonic peak ($\lambda_{1/2}$) gives reliable information about the particle size following the equation (with $\lambda_{1/2}$ in nm and diameter $D$ in Å):

$$1240 = \lambda_{1/2}\left[3.301 + \frac{294}{D^2} + \frac{1.09}{D}\right]$$

The value for the diameter ($D$) for a given ZnO/HBP was found to be ∼4 nm, which is in good agreement with the values obtained by particle size counts of TEM micrographs.

The TEM images show that the polymer plays an important role in the stabilization of ZnO NPs. In fact, in the absence of HYPAM$_x$-C$_{18}$-PEG$_{750}$ polymer two observations can be mentioned; a) a solution (3 g L$^{-1}$ in THF) of

(22) Verges, M. A.; Mifsud, A.; Serna, C. J. *J. Chem. Soc., Faraday Trans.* **1990**, *86*(6), 959–963.

(23) Meulenkamp, E. A. *J. Phys. Chem. B* **1998**, *102*(29), 5566–5572.

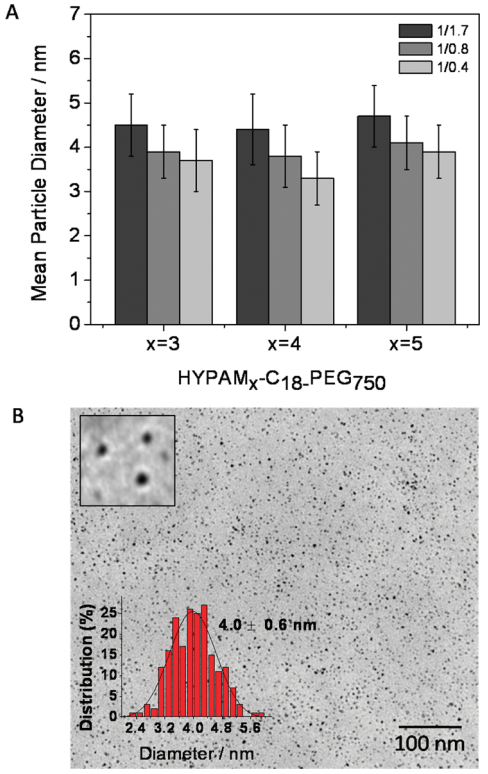


**Figure 4.** (A) Comparison of particle sizes for varying molar ratios of polymer/zinc precursor for the three generations of HBPs. (B) Typical TEM micrograph and histogram for a HYPAM$_5$-C$_{18}$-PEG$_{750}$/ZnO nanocomposite (weight ratio: 1/0.4) illustrating NPs of around 4.0 nm (ca. 300 nanoparticles analyzed). The inset (top left) is a micrograph of the negatively stained sample (using 1% uranyl acetate solution) showing the polymer (white ring) localized around a ZnO nanoparticle.

ZnO is visibly nonhomogeneous (contains white precipitate), and b) large aggregates of ZnO particles are observed in TEM. However, if the same quantity of ZnO, in the same THF solvent, is added to an equivalent of polymer (polymer/ZnO weight ratio of 1/2.1), a homogeneous clear solution is obtained. No linear trends in particle diameter were observed when comparing systems consisting of different HYPAM$_x$ generations ($x$ = 3, 4, or 5) and constant quantity of zinc precursor. This leads to the conclusion that the polymer-core sizes investigated in our case does not have a direct effect on the morphology of the nanoparticles grown within. All ZnO/HBP composites displayed the same electron diffraction pattern in the electron microscope (see the Supporting Information, Figure S2). The first three diffraction rings corresponding to indices 100, 002, and 101 are clearly visible, demonstrating the high crystallinity of the ZnO nanoparticles.

DLS and negatively stained TEM were performed in order to characterize the morphology of the nanohybrids; particularly the distribution of the NPs within both the macromolecule and the colloid. In solution, the hydrodynamic diameter of these nanoobjects was found to be around 30 nm. The inset in Figure 4b displays a typical image obtained after negative staining of ZnO nanohybrids. No bare ZnO NPs were observed. The hybrid ZnO/polymer systems clearly showed to have core−shell morphology, the dark cores corresponding to the electron-dense ZnO NPs embedded into a circular, brighter polymer shell. All the data collected by $^1$H NMR, DLS, and TEM experiments demonstrate that the hyperbranched polymers were adsorbed on the surface of ZnO NPs.

As commonly encountered in literature, zinc oxide possesses intriguing luminescent properties in the visible region of the spectrum. We studied the photoluminescent (PL) properties of HYPAM$_x$-C$_{18}$-PEG$_{750}$-stabilized ZnO NPs. Indeed, all the synthesized powder composites were luminescent under a UV lamp (at 365 nm) after redispersion in a chosen solvent (vide infra). It is also noteworthy that the colloidal solutions remained visibly stable without any phase separation for weeks. Redispersion analysis will be discussed at a later stage in this account. All samples display similar absorption spectra, typically a strong absorption is observed up to around 355 nm ($\approx$ 3.49 eV) followed by a sharp decrease. This is characteristic for nanometric zinc oxide with a band gap approximately at 365 nm ($\approx$ 3.4 eV). The PL properties of HYPAM$_5$-C$_{18}$-PEG$_{750}$-stabilized ZnO NPs (polymer/[Zn(Cy)$_2$] ratio:1/0.4) were investigated on a spectrofluorometer and displayed in Figure 5. A broad emission band in the visible region was observed for all samples. This yellow emission was centered at 575 nm for an excitation wavelength between 300 and 360 nm ($\approx$ 4.13 to 3.44 eV) and is well-known for ZnO nanoparticles. The origin of this emission is attributed to the recombination of a shallowly trapped electron with a deeply trapped hole. This photogenerated hole is due to surface defects such as oxygen vacancies in the structure.[24] The same figure also shows the characteristic excitation spectrum recorded for an emission wavelength of 580 nm ($\approx$ 2.14 eV) with a strong absorption below 355 nm ($\approx$ 3.49 eV), which is in agreement with the absorption spectrum. The quantum yield (QY) for a HYPAM$_3$-C$_{18}$-PEG$_{750}$-stabilized ZnO system was found to be 5%. This value is lower than some reported,[10,13a] and efforts are being made in QY improvement with the development of new hyperbranched polymers.

## 3. Stabilization Properties

From previous experiments, it was deduced that polymers of the type HYPAM$_x$-C$_{18}$-PEG$_{750}$ do interact with ZnO NPs. This was demonstrated more clearly by drying THF solutions of ZnO NPs in the presence of HYPAM$_x$-C$_{18}$-PEG$_{750}$. The resulting powder was easily redispersed in a wide range of solvents (see Figure 6): water, toluene, ethanol, dichloromethane, THF, and acetonitrile. UV−visible spectra of the solutions in different solvents were very similar. No significant changes in the photoluminescent properties of solutions containing nanoparticles were observed over a period of several weeks. This implies long-term colloidal stability, mainly induced by the intrinsic properties of the outer shell made of poly(ethylene glycol) polymer chains.

The stability of ZnO NPs in water was of special interest and thus the colloidal stability of ZnO/HBP hybrids in aqueous solutions were then investigated. Whatever the

(24) van Dijken, A.; Meulenkamp, E. A.; Vanmaekelbergh, D.; Meijerink, A. *J. Lumin.* **2000**, *90*(3−4), 123–128.

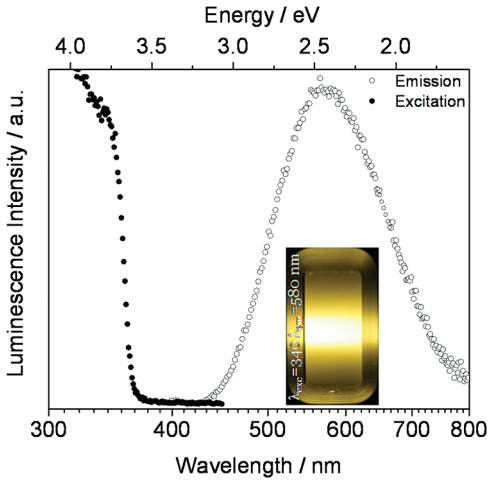


**Figure 5.** Spectrum for the yellow emission recording (circles) for a solution of $HYPAM_5$-$C_{18}$−$PEG_{750}$/ZnO nanocomposite (ratio: 1/0.4) in THF ($\lambda_{exc}$ = 340 nm) and corresponding excitation recording (full circle) for an emission of 580 nm. Inset: photo of yellow emission for $\lambda_{exc}$ = 340 nm.

molecular weight of the hyperbranched polymeric core, $HYPAM_3$, $HYPAM_4$ or $HYPAM_5$, or the polymer/$[Zn(Cy)_2]$ weight ratio (in the range studied here) may be, the colloidal stability of the final NP/polymer system in water was found to be very similar. First, DLS measurements highlighted the fact that a given nanohybrid tends to form large aggregates with hydrodynamic diameters of around 100−150 nm for concentrations above 0.1 g $L^{-1}$ (a tendency that has already been observed for the hyperbranched polymer alone, vide supra). Isolated objects with $D_h$ = 30 nm were only observed at more dilute concentrations. Moreover, nanohybrids remained stable over time and also after increasing the ionic strength of the solution by addition of NaCl up to a concentration of 1 mol $L^{-1}$. In addition, NPs remained stable for a wide range of pH values (from pH 5 to 12). Very low pH values induced the dissolution of ZnO NPs, whereas pH values higher than 12 led to partial hydrolysis of the ester and amide groups belonging to the hyperbranched stabilizing polymer. These results demonstrate the crucial role of the terminal

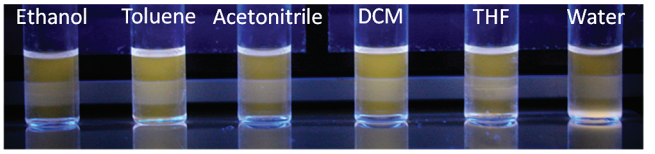


**Figure 6.** Photograph of luminescent $HYPAM_3$-$C_{18}$−$PEG_{750}$/ZnO nanocomposite (ratio 1/9), redispersed in several polar and apolar solvents under a UV lamp at 365 nm.

PEG chains as an external polar layer that provides excellent stabilization properties in water.

## Conclusion

The synthesis and characterization of a new family of dendritic polymers, comprising a hyperbranched polyamidoamine core with a core−shell or a core−multishell architecture based on PEG derivatives, has been described. The studies performed here clearly demonstrate the importance of the core−multishell architecture on the formation and stabilization of nanoparticles. Whereas the HYPAM core and inner shell allow strong interaction with the $[Zn(Cy)_2]$ precursor, the hydrophilic outer shell allows the easy dispersion and stabilization of ZnO NPs in water and organic solvents. We therefore believe that these multishell architectures can be used as potential nanoparticle stabilizers for biological applications, work that is currently under investigation.

**Acknowledgment.** This work has been supported and financed by the Centre National de la Recherche Scientifique (CNRS) together with the European Marie Curie Project NANOTOOL (MEST-CT-2005-020195). R.H. is thankful to the NanoFutur award from the German Ministry of Science (BMBF).

**Supporting Information Available:** $^1$H NMR of $HYPAM_4$ and $HYPAM_4$-$C_{18}$-$PEG_{750}$ and electron diffraction pattern for $HYPAM_3$-$C_{18}$-$PEG_{750}$/ZnO nanohybrids (PDF). This material is available free of charge via the Internet at http://pubs.acs.org.